SARS-CoV-2 Omicron spike mediated immune escape, infectivity and cell-cell fusion

Bo Meng[1,2#], Isabella A.T.M Ferreira[1,2#], Adam Abdullahi[1,2#], Akatsuki Saito[3#], Izumi Kimura[4#], Daichi Yamasoba[5#], Steven A. Kemp[1,2], Niluka Goonawardane[1,2], Guido Papa[6], Saman Fatihi[7], Surabhi Rathore[7], Terumasa Ikeda[5], Mako Toyoda[8], Toong Seng Tan[9], Jin Kuramochi[9], Shigeki Mitsunaga[10], Takamasa Ueno[8], Oscar J[12]. Charles[5], CITIID-NIHR BioResource COVID-19 Collaboration, The Genotype to Phenotype Japan (G2P-Japan) Consortium, Ecuador-COVID19 Consortium, Kenneth G.C. Smith[1,2], John Bradley[2], Jinwook Choi[13], Elo Madissoon[14,15], Kerstin Meyer[14], Petra Mlcochova[1,2], Rainer Doffinger[2], Sarah A. Teichmann[14, 16], Leo James[3], Joo Hyeon Lee[13,17], Lipi Thukral[7], Kei Sato[4,18]*, Ravindra K. Gupta[1,2,19]*

[1] Cambridge Institute of Therapeutic Immunology & Infectious Disease (CITIID), Cambridge, UK.

[2] Department of Medicine, University of Cambridge, Cambridge, UK.

[3]Department of Veterinary Science, Faculty of Agriculture, University of Miyazaki, Miyazaki 8892192, Japan

[4]Division of Systems Virology, Department of Infectious Disease Control, International Research Center for Infectious Diseases, The Institute of Medical Science, The University of Tokyo, Tokyo, 1088639, Japan

[5]Division of Molecular Virology and Genetics, Joint Research Center for Human Retrovirus infection, Kumamoto University, Kumamoto 8600811, Japan

[6] MRC – Laboratory of Molecular Biology, Cambridge, UK.

[7] CSIR Institute of Genomics and Integrative Biology, Delhi, India

[8]Division of Infection and Immunity, Joint Research Center for Human Retrovirus infection, Kumamoto University, Kumamoto 8600811, Japan

[9]Kuramochi Clinic Interpark, Utsunomiya, Tochigi 3210114, Japan

[10] Human Genetics Laboratory, National Institute of Genetics, Mishima, Shizuoka 4118540, Japan

[11] Department of Hematology and Oncology, Graduate School of Medicine, Kyoto University, Kyoto 6068507, Japan

[12]Division of Infection and Immunity, UCL, London

[13]Wellcome-MRC Cambridge Stem Cell Institute, Cambridge, UK.

[14]Wellcome Sanger Institute, Wellcome Genome Campus, Hinxton, Cambridge, UK

[15] European Molecular Biology Laboratory, European Bioinformatics Institute, EMBL-EBI, Wellcome Trust Genome Campus, Hinxton CB10 1SD, UK

[16]Cavendish Laboratory/Dept Physics, University of Cambridge, JJ Thomson Ave, Cambridge CB3 0HE, UK.

[17]Department of Physiology, Development and Neuroscience, University of Cambridge, Cambridge, UK.

[18]CREST, Japan Science and Technology Agency, Saitama 3220012, Japan

[19]Africa Health Research Institute, Durban, South Africa.

[#]Equal contribution.

*Address for correspondence:

rkg20@cam.ac.uk; keisato@g.ecc.u-tokyo.ac.jp

Key words: SARS-CoV-2; COVID-19; Omicron variant; B.1.1.529; antibody escape; neutralising antibodies; infectivity; spike mutation; evasion; resistance; fitness; fusion; syncytia, TMPRSS2, ACE2, ChAdOx-1, BNT162b.

Abstract

The SARS-CoV-2 Omicron BA.1 variant emerged in late 2021 and is characterised by multiple spike mutations across all spike domains. Here we show that compared to the Delta variant, Omicron BA.1 confers very significant evasion of therapeutic monoclonal and vaccine-elicited polyclonal neutralising antibodies after two doses. mRNA vaccination as a third vaccine dose rescues and broadens neutralisation in the short term. Importantly, antiviral drugs remdesevir and molnupiravir retain efficacy against Omicron BA.1. Despite three mutations predicted to favour spike S1/S2 cleavage, observed cleavage efficiency is substantially lower than for Delta. Omicron spike pseudotyped virus (PV) entry into lower airway organoids and Calu-3 lung cells was impaired. This defect for Omicron, but not Delta spike PV, correlated with higher cellular expression of TMPRSS2 transcripts, as determined by single cell RNA seq. Indeed we showed that in lung cells expressing TMPRSS2, live Omicron virus demonstrated significantly lower replication in comparison to Delta. This phenotype was reflected in cells where TMPRSS2 expression could be manipulated, with Omicron showing no change in entry in the presence of TMPRSS2. Cell-cell fusion mediated by spike glycoprotein is known require S1/S2 cleavage, but is also dependent on presence of TMPRSS2; fusogenicity of the Omicron BA.1 spike was severely impaired despite TMPRSS2 expression, leading to marked reduction in syncytium formation compared to Delta spike. These *in vitro* data indicate that suboptimal Omicron S1/S2 cleavage reduces efficient infection of lower airway cells expressing TMPRSS2, but not TMPRSS2 negative cells such as those found in the upper airway. Overall, Omicron appears to have gained significant immune evasion properties whilst modulating virus-cell interactions that alter tropism with implications for *in vivo* disease progression and transmission.

Introduction

The SARS-CoV-2 Omicron variant was first detected in South Africa and has now spread internationally[1]. It has been associated with very rapid increases in case numbers and recent data demonstrate significant evasion of neutralising antibody responses[1,2]. Omicron appears to be competing with the Delta variant in the UK, and this may be due to an advantage in vaccinated / previously exposed populations and/or increased replication (UKHSA technical report 32, Dec 17th). In contrast to immune evasion, data on replication and cell entry

efficiency are limited. Delta spike was previously shown to confer more efficient cell-cell fusion kinetics compared to Wuhan-1[3], and syncytia formation has previously been associated with pathogenesis[4]. Omicron has three mutations in the furin cleavage site region (P681H, H655Y and N679K) and was initially predicted to be highly infectious[5], fit and able to induce cell-cell fusion[6].

Here we show that as expected from mutational profiling, Omicron has significantly reduced sensitivity to neutralising monoclonal antibodies in clinical use and vaccine elicited antibodies in sera. However, contrary to predictions based on mutational profiling of the S1/2 cleavage region, Omicron spike is relatively poorly cleaved, and shows impaired entry and replication in lung cells expressing TMPRSS2, a serine protease enriched in lung alveolar type 1 and 2 cells. This reduced cleavage is also associated with poorer cell-cell fusion and syncytia formation, and these characteristics raise the possibility of altered pathogenesis.

Results

SARS-CoV-2 Omicron spike protein mutations across antigenic and cleavage domains

We first sought to investigate the distribution of mutations and their impacts. The Omicron variant carries 36 mutations in spike protein, with a high number of mutations occurring in the S1 region (Supplementary Figure 1a). While S2 subunit is relatively conserved and the Omicron variant harbours 6 unique mutations in S2 (N764K, D796Y, N856K, Q954H, N969K, L981F) that were not previously detected in other variants of concern. A combination of 25 substitutions exists on the adjacent N-terminal domain (NTD) and receptor binding domain (RBD), which are the main target for neutralising antibodies. We observed a dense intramolecular interaction network in the Delta and Omicron as compared to the Wu-1 (Supplementary Figure 1b). Interestingly, 6 unique salt-bridges were observed in the Omicron spike, two in the NTD (156GLU-14GLN and 228ASP-41LYS), one in the RBD region (535LYS-583GLU), one around the S1/S2 proteolytic cleavage site (679LYS-654GLU), and two proximal to the fusion peptide (780GLU-776LYS and 764LYS-737ASP). However, reduced hydrogen bonding within NTD of the Omicron variant was observed due to 3 major deletions (Δ69-70, Δ143-145, Δ211). These findings imply subtle changes in omicron non-covalent interactions with possible impact on host receptor binding.

In addition, when we analysed interactions with ACE2, Omicron BA.1 displayed multiple contacts at the binding interface in contrast to Delta and Wu-1 (Supplementary Figure 2a). In total, we found 9 hydrogen bonds between RBD and ACE2 residues including a salt bridge formed at the site of mutation between R496-D38. There was again a striking difference between electrostatics of Omicron and earlier variants, in particular with positive charge accumulating on the NTD surface (Supplementary Figure 2b). Notably, substitution of Gly142 into Asp142 and insertion of "EPE" patch after R214 along with Gly339Asp creates a dense negatively charged surface. On the other hand, the mutations around the RBD region mostly changed into positively charged residues (N440K, T478K, Q493R, Q498R, Y505H and T547K) which might impact the binding interface of ACE2 by favouring electrostatic interactions.

Another prominent region displaying altered accessible mutation sites is the furin cleavage site. Structurally, the loop containing the S1/S2 proteolytic cleavage site is largely flexible and extends outwards, exposing the cleavage site for fusion activity in both Delta and Omicron models (Supplementary Figure 2c). Further, in the case of omicron three mutations H655Y, N679K and P681H are found within 2 nm of each other at the S1/S2 site. A substitution at site Pro681 is also present in case of delta but with a different amino acid change to arginine. From molecular dynamics simulations, the loop was observed to have an overall reduced surface accessibility in Delta as compared to Omicron as it is oriented towards the protein.

Omicron escapes from a widely used therapeutic monoclonal antibody cocktail

Current standard of care antiviral treatment for moderate to severe COVID-19 includes use of the monoclonal antibody combination casivirimab and imdevimab (REGN 10933 and 10897 respectively). In the absence of clinical data for efficacy of these treatments against Omicron, we first modelled the interaction surface between each antibody and Omicron spike (Figure 1c). The E484A and Q493R changes were predicted to impact interations with casivirimab and S375F with imdevimab. Using live Delta and Omicron viruses we next tested component mAbs, both individually and in combination (Figure 1d). Whilst the Delta variant was effectively neutralised by casivirimab, imdevimab was partially effective, consistent with previous data Delta variant using pseudotyped virus[7]. The combination was highly potent against Delta in our live virus experiments. However, there was complete loss of neutralising activity against Omicron variant viruses by either mAb or the combination (Figure 1d). Given

these results, we next tested direct acting antivirals remdesivir and the active metabolite of molnupiravir against live Omicron virus. We observed similar inhibitory activity across Delta and Omicron viruses for both compounds (Supplementary Figure 3).

Omicron spike protein confers broad escape from two dose vaccination

A critical question is whether vaccine elicited antibodies are able to neutralise Omicron. In order to examine longitudinal changes in neutralisation in prospectively recruited participants, we used codon optimised spike expression plasmids for Omicron and Delta spike proteins and generated PV particles. We obtained longitudinal serum samples from individuals vaccinated with either BNT162b2 or ChAdOx-1 vaccines. We observed ≥ 10-fold loss of neutralisation against Omicron after the second dose compared to Delta. Indeed neutralisation of Omicron was not detectable for the majority of individuals who had received two doses of ChAdOx-1. We additionally also observed waning over time since second dose (Figure 3). Both groups were boosted with BNT162b2 as a third dose, allowing us to compare the response to this boosting dose. Similar magnitude increases in neutralisation were observed for all variants tested, suggesting increased breadth of responses as well as titre.

To confirm loss of neutralising activity against Omicron, we next used a live virus experimental system to compare Delta and Omicron isolates against sera taken four weeks after the second dose of BNT162b2, with similar results as obtained in the PV assay (Supplementary Figure 4a). These live virus isolates were also used to assess the neutralisation of the Omicron variant by sera derived from non-vaccinated individuals previously infected with the early Wuhan-1 virus, or the Delta variant. As expected, vaccine sera had significantly impaired activity against Omicron as compared to Delta (Supplementary Figure 4b). We also tested mRNA 1273 which showed similar neutralisation loss against Omicron variant as BNT162b2. Coronavac however showed little neutralisation against Delta and 0/9 participants had detectable neutralisation against our Omicron virus isolate. Interestingly sera from Delta infections appeared to have lower cross neutralisation as compared to those from the early pandemic period when Wuhan-1 D614G was dominant.

Omicron Spike protein mediates deficient cell entry and replication in lower airway cells expressing TMPRSS2

Spike mediates cell entry via interaction with ACE2 and TMPRSS2[8] and is a major determinant of viral infectivity. The plasma membrane route of entry, and indeed transmissibility in animal models, is critically dependent on the polybasic cleavage site (PBCS) between S1 and S2[5,9,10] and cleavage of spike prior to virion release from producer cells; this contrasts with the endosomal entry route, which does not require spike cleavage in producer cells [5,6,11]. Plasma membrane fusion additionally allows the virus to avoid restriction factors in endosomes[5].

We tested viral entry of WT Wuhan-1 D614G, Delta and Omicron spikes (Figure 2a) using the PV system. We first probed PV virions for spike protein and noted around four fold reduced Omicron spike incorporation into virions, in contrast to Delta and WT (Figure 2b,c). We also noted that the Omicron spike was predominantly in the uncleaved form, in contrast to Delta and WT (Figure 2b,d). Of note cleavage of Omicron spike in cells was also lower compared to Delta and WT (Figure 2e-f), as can be seen from faint S2 and S1 bands after probing with S2 and S1 antibodies respectively. We next infected primary 3D lower airway organoids[12,13] (Figure 2g) and Calu-3 lung cells (Figure 2h) expressing endogenous levels of ACE2 and TMPRSS2. We observed variable entry efficiency for Omicron in comparison to Delta and Wuhan-1 D614G wild type. SARS-CoV-2 infection in organoids and Calu-3 lung cells was impaired for Omicron relative to Delta and Wuhan D614G. By contrast, in H1299 lung epithelial cells we observed similar entry efficiency for Delta and Omicron (Figure 2i). Finally, we infected Calu-3 cells with live SARS-CoV-2 Omicron virus, and observed more than 10 fold greater viral RNA in supernatants at 24 and 48 hours (Figure 2j).

TMPRSS2 levels differ across lung cells and are higher in lower airway cells

In order to explore our PV entry and infection findings, we further studied the expression of ACE2 and TMPRSS2 in non-small cell lung cancer epithelial cell lines H1299 and Calu-3[14]. Single-cell RNA-seq data showed higher expression of both ACE2 and TMPRSS2 in Calu-3 than in the H1299 (Figure 3a). To further probe the dependence on TMPRSS2 on virus entry, we transduced/infected 293T cells overexpressing either ACE2 and TMPRSS2 (A2T2) or ACE2 only with TMPRSS2 being knocked out (A2ΔT2)[9]. Enhanced infectivity was observed from both WT and Delta in the presence TMPRSS2 suggesting TMPRSS2 is additionally required for their optimal virus entry. In contrast, no difference was observed from Omicron PV indicating Omicron spike has lost its advantage in utilising TMPRSS2 for entry (Figure 3b).

Having established that TMPRSS2 could modulate entry mediated by Delta but not Omicron BA.1 spike, we sought to understand the distribution of TMPRSS2 expression in human respiratory cells; we used single-nuclei RNA-seq data from 5 locations in the human lung[15]. The comparison of alveolar and airway epithelial cells revealed higher expression of TMPRSS2 in the alveolar AT1 and AT2 pneumocytes, and in general lower expression in the trachea (upper airway, Figure 3c). ACE2 expression also appeared higher in AT1 and AT2 cells as compared to other cell types.

Omicron Spike protein induces relatively poor cell-cell fusion compared to Delta

Mutations at P681 in the PBCS have been observed in multiple SARS-CoV-2 lineages, most notably in the B.1.1.7 Alpha variant[16] and the Delta variant. We previously showed that these spikes, bearing P681 mutations, had significantly higher fusogenic potential than a D614G Wuhan-1 spike [6]. Omicron bears P681H, in addition to 679 and 655 mutations (**Figure 2a**). We tested the Omicron spike using a split GFP system to monitor cell-cell fusion in real time (**Figure 4a,b**). We transfected spike bearing plasmids into 293T cells expressing GFP1-10 and mixed with Vero cells stably expressing the GFP-11, so that the GFP signal could be detected upon cell-cell fusion and measured over time. (**Figure 4b,c**). We observed increased fusion for Delta as compared to D614G Wuhan-1 spike as shown previously. The Omicron spike however resulted in very poor fusion (**Figure 4c)**, despite being expressed (**Figure 2b**).

Discussion

Here we have shown that the Omicron spike confers very significant evasion of vaccine elicited neutralising antibodies that is more dramatic for ChAdOx-1 versus BNT162b2 vaccine sera. These data are supported by vaccine effectiveness measurements in the UK (UKHSA report Dec 2021). In longitudinally sampled participants, second dose waning was mitigated by third dose mRNA vaccination that also increased and broadened neutralisation of Omicron in the short term, though waning is likely to occur over time.

Critically, ChAdOx-1 is widely used in low income settings where third doses with mRNA not widely available, and Omicron may contribute to higher infection rates and severe disease in such settings unless mRNA third doses can be implemented. Of further concern for low income countries was the absence of any neutralising activity to Omicron in sera after two doses of Coronavac in all of nine participants, in addition to poor Delta neutralisation.

Neutralising antibodies elicited by previous infection were also compromised by Omicron and notably, infections due to Delta appeared to provide significantly lower Omicron neutralisation when compared to early 2020 sera.

In terms of Omicron BA.1 implications for treatment options for moderate to severe clinical disease, we show high level loss of *in vitro* activity for the widely used mAb combination therapy REGN2, but no significant loss of activity of the polymerase inhibitors remdesivir and molnupiravir against live virus. The mAb sotrovimab has also been reported to retain significant *in vitro* activity against Omicron[17], though concerns regarding resistance exist around the use of a single agent.

Our molecular dynamic modelling studies had suggested a significantly re-arranged surface profile of the loop containing the PBCS in Omicron BA.1. Importantly, despite presence of three mutations predicted to favour spike S1/S2 cleavage, the observed cleavage efficiency is similar to wild type Wuhan-1 D614G and lower than Delta. Omicron spike was also associated with lower entry into target lower airway organoids or Calu-3 lung cells expressing TMPRSS2 in addition to ACE2. Our analysis of scRNA-seq data suggest that lung cells have higher ACE2 and TMPRSS2 mRNA as compared to upper airway cell types. Recent findings from Hong Kong suggest higher replication in ex vivo lung tissue as compared to upper airway tissue for Omicron, but not for Delta (HKU website). A mechanism for Omicron's poorer replication in the ex vivo tissue can be derived from our findings regarding reduced Omicron spike cleavage and poor utilisation of TMPRSS2 dependent plasma membrane fusion by Omicron spike.

As expected from suboptimal cleavage, and the fact that cell-cell fusion requires TMPRSS2, low fusogenic potential of the Omicron spike was observed when expressed in cells. This phenomenon could translate to impaired cell-cell spread, and indeed investigators have observed smaller plaque sizes (personal communication). These observations highlight that Omicron has gained immune evasion properties whilst compromising cell entry in lung cells and ability to form syncytia, with possible implications for pathogenicity. Further ex vivo and in vivo studies are urgently needed to test this hypothesis.

Methods

Serum samples and ethical approval

Ethical approval for study of vaccine elicited antibodies in sera from vaccinees was obtained from the East of England – Cambridge Central Research Ethics Committee Cambridge (REC ref: 17/EE/0025). Studies involving health care workers (including testing and sequencing of respiratory samples) were reviewed and approved by The Institutional Human Ethics Committees of NCDC and CSIR-IGIB(NCDC/2020/NERC/14 and CSIR-IGIB/IHEC/2020-21/01). Participants provided informed consent.

The virus isolation procedures in this study were approved by the Institutional Review Board of National Institute for Infectious Diseases (approval ID: 1178) and Tokyo Metropolitan Institute of Public Health (approval ID: 3KenKenKen-466) according to the Declaration of Helsinki 2013. All protocols involving specimens from human subjects recruited at Kyoto University, Kuramochi Clinic Interpark and Universidad San Francisco de Quito were reviewed and approved by the Institutional Review Boards of Kyoto University (approval ID: G0697), Kuramochi Clinic Interpark (approval ID: G2021-004) and Universidad San Francisco de Quito (approval ID: CEISH P2020-022IN), and the Ecuadorian Ministry of Health (approval IDs: MSP-CGDES-2020-0121-O and MSP-CGDES-061-2020). The export of sera from Ecuador to Japan was approved by ARCSA ID: ARCSA-ARCSA-CGTC-DTRSNSOYA-2021-1626-M. All human subjects provided written informed consent. All protocols for the use of human specimens were reviewed and approved by the Institutional Review Boards of The Institute of Medical Science, The University of Tokyo (approval ID: 2021-1-0416), Kumamoto University (approval IDs: 2066 and 2074), University of Miyazaki (approval ID: O-1021)

Sequencing

Spike genomes for the original Wuhan strain, and Omicron VOC were obtained from GISAID EpiCoV database accessed on 30th November 2021. A consensus Spike genome was created from all complete and high coverage genomes, excluding all sequences with >5% Ns using Geneious Prime v2022. The consensus genome was translated to poly-proteins and the Spike gene was aligned to the original Wuhan strain using mafft v7.490[18] with the --globalpair --maxiterate 1000 flags.

Structural analysis: *generation of Spike mutant models in supplementary figures*

The protein structure PDB ID 7A94 was taken as a reference structure to generate the wild-type spike model consisting of 1146 residues (Benton et al., 2020). The complex structure

depicts the 1-RBD-up conformation in spike protein, with the limited missing regions [71–75, 625–632, 677–688, 828–852, and 941–943] modeled using Modeller (Sali and Blundell, 1993). The hACE2 structure in the template also had six residues missing patches that were added by taking PDB ID 1R42 as a reference. The complete 1146 spike-hACE2 structural model was used as a template to create variant models using Dunbrack 2010 backbone-dependent rotamer library in Chimera (Shapovalov and Dunbrack Jr, 2011). Further processing of steps involving minimisation and peptide bond building (after deletions for B.1.617.2 and B.1.529 spike) were performed using Gromacs toolkit. The mutated structural models were subjected to minimization in vacuum for extensive sidechain minimization.

Molecular dynamics simulations:

ACE2-bound 1-RBD-up complex structures of WT, B.1.617.2 and B.1.529 were placed in a triclinic box. 8 Na+ ions were added to neutralize the B.1.529 (Omicron) and 16 Na+ for B.1.617.2 (Delta) . TIP3P water representation was used to solvate the system. The simulations were carried out using GROMACS version 2018.3 by employing the CHARMM36 all-atom force field (Abraham et al., 2015). Periodic boundary conditions were used and 1.2 nm was set as real space cut-off distance. Particle Mesh Ewald (PME) summation using the grid spacing of 0.16 nm was used in combination with a fourth-order cubic interpolation to deduce the forces and potential in-between grid points . The van der Waals cut-off was set to 1.2 nm. A 2 fs time step for numerical integration of the equations of motion was used and the coordinates were saved at every 100 ps. The initial systems were subjected to energy minimization using the steepest descent method. Temperature and pressure were maintained at 310 K and 1 bar using V-rescale thermostat and Parrinello-Rahman barostat, respectively. Simulations of both the Delta and Omicron systems were carried out for 100 ns each. All the molecular images were rendered using ChimeraX (Pettersen et al., 2021), and PyMOL (Schrödinger, LLC, 2015).

Structural analysis:

The 100 ns molecular dynamics trajectory for Delta and Omicron was utilised to obtain the intra-protein interactions analysis. The analysis was performed using Pyinteraph and the interaction plotter (pymol plugin) was used to map the interactions identified by Pyinteraph on the 3D-spike structure (Tiberti et al., 2014). The detailed methodology of the analysis can be found from our previous work (Fatihi et al., 2021). The potential distribution was

calculated by APBS and the charge distribution is shown with the values ranging from –1k*T*(red) to 0 (white) and to +1k*T* (blue), where *T* is the temperature, and k is the Boltzmann constant (Jurrus et. al, 2018).

Data availability:

The above structural models used in this study for Delta and Omicron variants are available at https://github.com/CSB-Thukral-Lab/Spike_structural_models_Delta_and_Omicron

3D structural models of the spike homotrimer protein complex were alternatively also generated using Alphafold v2.1.1[19]. In its validation at the 14th edition of the Critical Assessment of protein Structure Prediction (CASP14) the predictions generated were demonstrated to be comparative to experimental structures. When a close homolog structure is available to Alphafold the predictions it generates for those positions are within typical experimental error. Required databases were downloaded on 02/12/2021. The program was run with the parameters --max_template_date=2021-12-01 --model_preset=monomer --db_preset=full_dbs --is_prokaryote_list=false. Protein structures were visualised in ChimeraX v1.3[20]. As predicted structures for the whole spike protein include poorly resolved chains at the terminal ends, these residues were identified by overlaying structures on PDB entry 6ZP2, then selected and removed from PDB files using the delete atoms/bonds action. Two further monomers were overlayed on 6zp2 to generate a homotrimer structure. Mutated residues were then coloured in red and labelled manually with respect to the Wuhan strain.

To model interactions between the omicron spike RBD and REGN 10933 and 10987, 6XDG was downloaded from PDB and aligned to the alphafolded omicron spike using the matchermaker function in ChimeraX v1.3. Predicted hydrogen bonds were plot within ChimeraX using a relaxed distance of 0.400Å and are shown as dashed green and blue lines. Predicted contact points between the RBD and REGN 10933 and 10987chains are indicated as red spheres using the same criteria as for hydrogen bonds.

Data availability:

All protein structures shown are freely available at github.com/ojcharles/viral_alphafold

Pseudotype virus experiments

Cells

HEK 293T CRL-3216, Hela-ACE-2 (Gift from James Voss), Vero CCL-81 were maintained in Dulbecco's Modified Eagle Medium (DMEM) supplemented with 10% fetal calf serum (FCS), 100 U/ml penicillin, and 100mg/ml streptomycin. All cells were regularly tested and are mycoplasma free. H1299 cells were a kind gift from Simon Cook. Calu-3 cells were a kind gift from Paul Lehner, A549 A2T2[21] cells were a kind gift from Massimo Palmerini. Vero E6 Ace2/TMPRSS2 cells were a kind gift from Emma Thomson.

Pseudotype virus preparation for testing against vaccine elicited antibodies and cell entry

Plasmids encoding the spike protein of SARS-CoV-2 D614 with a C terminal 19 amino acid deletion with D614G were used. Omicron and Delta spikes were generated by gene synthesis. Viral vectors were prepared by transfection of 293T cells by using Fugene HD transfection reagent (Promega). 293T cells were transfected with a mixture of 11ul of Fugene HD, 1µg of pCDNAΔ19 spike-HA, 1ug of p8.91 HIV-1 gag-pol expression vector and 1.5µg of pCSFLW (expressing the firefly luciferase reporter gene with the HIV-1 packaging signal). Viral supernatant was collected at 48 and 72h after transfection, filtered through 0.45um filter and stored at -80˚C as previously described. Infectivity was measured by luciferase detection in target 293T cells transfected with TMPRSS2 and ACE2.

Standardisation of virus input by SYBR Green-based product-enhanced PCR assay (SG-PERT)

The reverse transcriptase activity of virus preparations was determined by qPCR using a SYBR Green-based product-enhanced PCR assay (SG-PERT) as previously described[22]. Briefly, 10-fold dilutions of virus supernatant were lysed in a 1:1 ratio in a 2x lysis solution (made up of 40% glycerol v/v 0.25% Triton X-100 v/v 100mM KCl, RNase inhibitor 0.8 U/ml, TrisHCL 100mM, buffered to pH7.4) for 10 minutes at room temperature.

Sample lysates (12 µl) were added to 13 µl of SYBR Green master mix (containing 0.5µM of MS2-RNA Fwd and Rev primers, 3.5pmol/ml of MS2-RNA, and 0.125U/µl of Ribolock RNAse inhibitor and cycled in a QuantStudio. Relative amounts of reverse transcriptase activity were determined as the rate of transcription of bacteriophage MS2 RNA, with absolute RT activity calculated by comparing the relative amounts of RT to an RT standard of known activity.

Neutralisation titre analyses

Neutralisation by vaccine-elicited antibodies after two doses of the BNT162b2 and Chad-Ox-1 vaccine, in addition to a third dose with BNT162b2 was determined by infections in the presence of serial dilutions of sera as described below. The ID50 within groups were summarised as a geometric mean titre (GMT) and statistical comparison between groups were made with Mann-Whitney or Wilcoxon ranked sign tests. Statistical analyses were performed using Stata v13 and Prism v9.

Western blotting

Cells were lysed and supernatants collected 18 hours post transfection. Purified virions were prepared by harvesting supernatants and passing through a 0.45 µm filter. Clarified supernatants were then loaded onto a thin layer of 8.4% optiprep density gradient medium (Sigma-Aldrich) and placed in a TLA55 rotor (Beckman Coulter) for ultracentrifugation for 2 hours at 20,000 rpm. The pellet was then resuspended for western blotting. Cells were lysed with cell lysis buffer (Cell signalling), treated with Benzonase Nuclease (70664 Millipore) and boiled for 5 min. Samples were then run on 4%–12% Bis Tris gels and transferred onto nitrocellulose or PVDF membranes using an iBlot or semidry (Life Technologies and Biorad, respectively).

Membranes were blocked for 1 h in 5% non-fat milk in PBS + 0.1% Tween-20 (PBST) at room temperature with agitation and probed with the following primary antibodies: anti-SARS-CoV-2 Spike which detects the S2 subunit of SARS-CoV-2 S (Invitrogen, PA1-41165), anti-GAPDH (proteintech) or anti-p24 (NIBSC)) diluted in 5% non-fat milk in PBST for 2 h at 4°C with agitation. Blots were washed four times in PBST for 5 min at room temperature and labelled with secondary anti-rabbit HRP (1:10000, Invitrogen 31462), and anti-bactin HRP (1:5000; sc-47778) antibodies diluted in 5% non-fat milk in PBST for 1 h with agitation at room temperature. Membranes were washed four times in PBST for 5 min at room temperature and imaged using a ChemiDoc MP system (Bio-Rad).

Analysis of single-nuclei and single-cell RNA sequencing datasets.

Normalised and log-transformed expression values per cell were obtained from human lung single-nuclei and epithelial non-small cell lung carcinoma cell lines. scanpy 1.7.1 was used to process the data. For the tissue data[15], only single-nuclei RNA-seq were selected. From the

cancer cell lines study, only mock samples were selected. ACE2 and TMPRSS2 expression was plotted with violin plot function in scanpy.

Plasmids for split GFP system to measure cell-cell fusion

pQCXIP□BSR□GFP11 and pQCXIP□GFP1□10 were from Yutaka Hata [23] Addgene plasmid #68716; http://n2t.net/addgene:68716; RRID:Addgene_68716 and Addgene plasmid #68715; http://n2t.net/addgene:68715; RRID:Addgene_68715)

Generation of GFP1□10 or GFP11 lentiviral particles

Lentiviral particles were generated by co-transfection of 293T or Vero cells with pQCXIP□BSR□GFP11 or pQCXIP□GFP1□10 as previously described [24]. Supernatant containing virus particles was harvested after 48 and 72 hours, 0.45 µm filtered, and used to infect 293T or Vero cells to generate stable cell lines. 293T and Vero cells were transduced to stably express GFP1□10 or GFP11 respectively and were selected with 2 µg/ml puromycin.

Cell-cell fusion assay

Cell-cell fusion assays were carried out as previously described [24,25] but using a Split-GFP system. Briefly, 293T GFP1-10 and Vero-GFP11 cells were seeded at 80% confluence in a 1:1 ration in 24 multiwell plate the day before. Cells. were co-transfected with 0.5 µg of spike expression plasmids in pCDNA3 using Fugene 6 and following the manufacturer's instructions (Promega). Cell-cell fusion was measured using an Incucyte and determined as the proportion of green area to total phase area. Data were then analysed using Incucyte software analysis. Graphs were generated using Prism 8 software.

Sera Collection for live virus neutralisation experiments

Vaccine sera were collected from fourteen vaccinees four weeks after the second vaccination with BNT162b2 (Pfizer-BioNTech) (average age: 46, range: 38-55, 21% male). The sera obtained from seven vaccinees 2-3 weeks after the second vaccination with ChAdOx1 (Oxford-AstraZeneca) (average age: 46, range: 35-54, 71% male) were purchased from BioIVT.

Convalescent sera were collected from ten vaccine-naive individuals who had been infected with Delta variant (AY.29) (average age: 46, range: 22-63, 70% male). To determine the

SARS-CoV-2 variants infected, saliva were collected from COVID-19 patients during onset and RNA was extracted using a QIAamp viral RNA mini kit (Qiagen, Qiagen, Cat# 52906) according to the manufacturer's protocol. The sample was subjected to whole genome sequencing based on a modified ARTIC Network protocol[26], and the near full-length SARS-CoV-2 genome sequences were obtained. Alternatively, we also performed the capture-hybridization method. The RNA isolated from saliva was treated with DNase I (Takara, Cat# EN0521) and the sequencing library was prepared using Twist library preparation kit (Twist Bioscience, Cat# 101058). The capture-hybridization was conducted using xGen COVID-19 capture panel and xGen hybridization and wash kit (Integrated DNA Technologies, Cat# 1080578) according to the manufacturer's instruction. Illumina sequencing was performed using MiSeq reagent kit v2 (300 cycles) and a MiSeq sequencer (Illumina). For the data analysis, trimmomatic-0.39 (reference[27]) was used to remove the adaptors and low-quality reads from the raw sequence data. The trimmed paired-end reads were aligned to the human genome hg38 using bowtie2 v2.3.4.3 (reference[28]) and unmapped reads were mapped to the original SARS-CoV-2 genome (strain Wuhan-Hu-1, GenBank accession no. NC_045512.2) using Bwa-mem2 (https://github.com/bwa-mem2/bwa-mem2). The PCR duplicates were removed by gencore v0.16.0 (reference [29]) and a consensus sequence was obtained by IGV v2.10.2 (reference [30]). The mutations detected and viral lineage were determined by using CoVsurver (https://corona.bii.a-star.edu.sg) and Pangolin COVID-19 lineage assigner (https://pangolin.cog-uk.io/). The twelve convalescent sera during early pandemic (until April 2020) (average age: 71, range: 52-92, 8% male) were purchased from RayBiotech. Sera were inactivated at 56°C for 30 min and stored at –80°C until use.

Cell Culture for live virus experiments

HOS-ACE2/TMPRSS2 cells (HOS cells stably expressing human ACE2 and TMPRESS2)[4,31] were maintained in Dulbecco's modified Eagle's medium (high glucose) (Wako, Cat# 044-29765) containing 10% foetal bovine serum (FBS) and 1% PS. VeroE6/TMPRSS2 cells [an African green monkey (*Chlorocebus sabaeus*) kidney cell line; JCRB1819][32] were maintained in Dulbecco's modified Eagle's medium (low glucose) (Wako, Cat# 041-29775) containing 10% FBS, G418 (1 mg/ml; Nacalai Tesque, Cat# G8168-10ML) and 1% PS. Calu-3 cells (a human lung epithelial cell line; ATCC HTB-55) were maintained in Eagle's minimum essential medium (Sigma-Aldrich, Cat# M4655-500ML) containing 10% FBS and 1% PS.

SARS-CoV-2 live virus isolation, preparation and titration

To isolate an Omicron variant (BA.1 lineage, strain TY38-873; GISAID ID: EPI_ISL_7418017), saliva was collected from a traveller arrived at Japan, and quantitative RT-PCR testing for SARS-CoV-2 was performed in an airport quarantine station, Japan. The sample was subjected to whole genome sequencing based on a modified ARTIC Network protocol[26], and the near full-length SARS-CoV-2 genome sequence (GISAID ID: EPI_ISL_6913953) was deposited in GISAID. Virus isolation was performed as previously described[32]. In brief, the saliva was inoculated into VeroE6/TMPRSS2 cells and cytopathic effect (CPE) was observed 4 days after inoculation. The supernatant was then harvested and stored at –80°C as an original virus (GISAID ID: EPI_ISL_7418017). After one more passage in VeroE6/TMPRSS2 cells, the virus was obtained from National Institute of Infectious Diseases, Japan. A D614G-bearing early pandemic isolate (B.1.1lineage, strain TKYE610670; GISAID ID: EPI_ISL_479681) and a Delta isolate (B.1.617.2 lineage, strain TKYTK1734; GISAID ID: EPI_ISL_2378732) were used in the previous study[4].

Virus preparation and titration was performed as previously described[4,31]. To prepare the working virus stock, 100 µl of the seed virus was inoculated into VeroE6/TMPRSS2 cells (5×10^6 cells in a T-75 flask). One hour after infection, the culture medium was replaced with Dulbecco's modified Eagle's medium (low glucose) (Wako, Cat# 041-29775) containing 2% FBS and 1% PS. At 3 days postinfection, the culture medium was harvested and centrifuged, and the supernatants were collected as the working virus stock.

The titre of the prepared working virus was measured as the 50% tissue culture infectious dose ($TCID_{50}$). Briefly, one day prior to infection, VeroE6/TMPRSS2 cells (10,000 cells/well) were seeded into a 96-well plate. Serially diluted virus stocks were inoculated into the cells and incubated at 37°C for 4 days. The cells were observed under microscopy to judge the CPE appearance. The value of $TCID_{50}$/ml was calculated with the Reed–Muench method as previously described[7].

SARS-CoV-2 Infection with live virus

One day prior to infection, Calu-3 cells (10,000 cells) were seeded into a 96-well plate. SARS-CoV-2 (1,000 $TCID_{50}$ as measured with plaque assay on Vero cells) was inoculated and incubated at 37°C for 1 h. The infected cells were washed, and 180 µl of culture medium was added. The culture supernatant (10 µl) was harvested at the indicated time points and used for real-time RT-PCR to quantify viral RNA copy number (see below).

Real-Time RT-PCR

Real-time RT-PCR was performed as previously described[4,31]. Briefly, 5 μl of culture supernatant was mixed with 5 μl of 2 × RNA lysis buffer [2% Triton X-100, 50 mM KCl, 100 mM Tris-HCl (pH 7.4), 40% glycerol, 0.8 U/μl recombinant RNase inhibitor (Takara, Cat# 2313B)] and incubated at room temperature for 10 min. RNase-free water (90 μl) was added, and the diluted sample (2.5 μl) was used as the template for real-time RT-PCR performed according to the manufacturer's protocol using the One Step TB Green PrimeScript PLUS RT-PCR kit (Takara, Cat# RR096A) and the following primers: Forward *N*, 5'-AGC CTC TTC TCG TTC CTC ATC AC-3'; and Reverse *N*, 5'-CCG CCA TTG CCA GCC ATT C-3'. The viral RNA copy number was standardized with a SARS-CoV-2 direct detection RT-qPCR kit (Takara, Cat# RC300A). Fluorescent signals were acquired using a QuantStudio 3 Real-Time PCR system (Thermo Fisher Scientific), a CFX Connect Real-Time PCR Detection system (Bio-Rad), an Eco Real-Time PCR System (Illumina) or a 7500 Real Time PCR System (Applied Biosystems).

Preparation of Monoclonal Antibodies

Casirivimab and Imdevimab were prepared as previously described[33]. To construct the plasmids expressing anti-SARS-CoV-2 monoclonal antibodies (Casirivimab and Imdevimab), the sequences of the variable regions of Casirivimab and Imdevimab were obtained from KEGG Drug Database (https://www.genome.jp/kegg/drug/) and were artificially synthesized (Fasmac). The obtained coding sequences of the variable regions of the heavy and light chains were cloned into the pCAGGS vector containing the sequences of the human immunoglobulin 1 and kappa constant region [kindly provided by Dr. Hisashi Arase (Osaka University, Japan)].

To prepare these monoclonal antibodies, the pCAGGS vectors containing the sequences encoding the immunoglobulin heavy and light chains were cotransfected into HEK293T cells using PEI Max (Polysciences, Cat# 24765-1). At 48 h posttransfection, the cell culture supernatants were harvested, and the antibodies were purified using NAb protein A plus spin kit (Thermo Fisher Scientific, Cat# 89948) according to the manufacturer's protocol.

Neutralisation Assay with live virus

One day prior to infection, VeroE6/TMPRSS2 (10,000 cells) were seeded into a 96-well plate. The monoclonal antibodies (Casirivimab, Imdevimab, or Casirivimab/Imdevimab) and

the heat-inactivated human sera were serially diluted with DMEM supplemented with 10% FCS and 1% PS. The diluted antibodies and sera were incubated with SARS-CoV-2 (120 $TCID_{50}$) at 37°C for 1 h. The viruses without antibodies or sera were included as controls. The mixture (containing the virus at 100 $TCID_{50}$) was inoculated onto a monolayer of VeroE6/TMPRSS2 cells and incubated at 37°C for 1 h. Then, the cells were washed with DMEM and cultured in DMEM supplemented with 10% FCS and 1% PS. At 24 h postinfection, the culture supernatants were harvested and viral RNA was quantified by real-time RT-PCR (see above). The assay of each antibody or serum was performed in triplicate or quadruplicate, and the 50% neutralization titre was calculated using Prism 9 (GraphPad Software).

Antiviral drug assay with live virus

One day prior to infection, HOS-ACE2-TMPRSS2 cells (10,000 cells) were seeded into a 96-well plate. The cells were infected with SARS-CoV-2 (100 $TCID_{50}$) at 37°C for 1 h. Then, the cells were washed with DMEM and cultured in DMEM supplemented with 10% FCS and 1% PS and the serially diluted Remdesivir (Selleck, Cat# S8932) or beta-d-N4-hydroxycytidine (a derivative of Molnupiravir; Cell Signaling Technology, Cat# 81178S). At 24 h postinfection, the culture supernatants were harvested and viral RNA was quantified by real-time RT-PCR (see above). The assay of each compound was performed in quadruplicate, and the 50% neutralization titre was calculated using Prism 9 (GraphPad Software).

Cytotoxicity Assay

The CPE of the Remdesivir and beta-d-N4-hydroxycytidine were tested using a cell counting kit-8 (Dojindo, Cat# CK04-11) according to the manufacturer's instructions. One day prior to the assay, HOS-ACE2-TMPRSS2 cells (10,000 cells) were seeded into a 96-well plate. The cells were cultured with the serially diluted compound for 24 hours. The cell counting kit-8 solution (10 µl) was added to each well, and the cells were incubated at 37°C for 90 m. Absorbance was measured at 450 nm by GloMax explorer microplate reader (Promega).

Acknowledgments

RKG is supported by a Wellcome Trust Senior Fellowship in Clinical Science (WT108082AIA). This study was supported by the Cambridge NIHRB Biomedical Research Centre. I.A.T.M.F. is funded by a SANTHE award (DEL-15-006). We would like to thank Paul Lehner for Calu-3 cells. We would like to thank James Voss for HeLa ACE2 and

Suzanne Rihn for the A549 cells. Davide Corti for the Omicron spike plasmid. We thank the Geno2pheno UK consortium. The authors acknowledge support from the G2P-UK National Virology consortium funded by MRC/UKRI (grant ref: MR/W005611/1).This study was also supported by The Rosetrees Trust and the Geno2pheno UK consortium. SF acknowledges the EPSRC (EP/V002910/1). KS is supported by AMED Research Program on Emerging and Re-emerging Infectious Diseases (20fk0108270 and 20fk0108413), JST SICORP (JPMJSC20U1 and JPMJSC21U5) and JST CREST (JPMJCR20H4). We would like to thank all members belonging to The Genotype to Phenotype Japan (G2P-Japan) Consortium. We thank National Institute for Infectious Diseases, Japan and Hisashi Arase (Osaka University, Japan) for providing virus isolates and reagents and Ituro Inoue and Sachiko Sakamoto (National Institute of Genetics, Japan) for technical supports. This study was supported in part by AMED Research Program on Emerging and Re-emerging Infectious Diseases 20fk0108163 (to Akatsuki Saito), 20fk0108146 (to Kei Sato), 20fk0108270 (to Kei Sato), 20fk0108413 (to Terumasa Ikeda and Kei Sato) and 20fk0108451 (to Akatsuki Saito, Terumasa Ikeda, Takamasa Ueno, Akifumi Takaori-Kondo, G2P-Japan Consortium and Kei Sato); AMED Research Program on HIV/AIDS 21fk0410033 (to Akatsuki Saito) and 21fk0410039 (to Kei Sato); AMED Japan Program for Infectious Diseases Research and Infrastructure 20wm0325009 (to Akatsuki Saito) and 21wm0325009 (to Akatsuki Saito); JST A-STEP JPMJTM20SL (to Terumasa Ikeda); JST SICORP (e-ASIA) JPMJSC20U1 (to Kei Sato); JST SICORP JPMJSC21U5 (to Kei Sato), JST CREST JPMJCR20H4 (to Kei Sato); JSPS KAKENHI Grant-in-Aid for Scientific Research C 19K06382 (to Akatsuki Saito), Scientific Research B 18H02662 (to Kei Sato) and 21H02737 (to Kei Sato); JSPS Fund for the Promotion of Joint International Research (Fostering Joint International Research) 18KK0447 (to Kei Sato); JSPS Core-to-Core Program JPJSCCA20190008 (A. Advanced Research Networks) (to Kei Sato); JSPS Research Fellow DC1 19J20488 (to Izumi Kimura); JSPS Leading Initiative for Excellent Young Researchers (LEADER) (to Terumasa Ikeda); Takeda Science Foundation (to Terumasa Ikeda); The Tokyo Biochemical Research Foundation (to Kei Sato); Mitsubishi Foundation (to Terumasa Ikeda); Shin-Nihon Foundation of Advanced Medical Research (to Terumasa Ikeda); a Grant for Joint Research Projects of the Research Institute for Microbial Diseases, Osaka University (to Akatsuki Saito) ; an intramural grant from Kumamoto University COVID-19 Research Projects (AMABIE) (to Terumasa Ikeda); Intercontinental Research and Educational Platform Aiming

for Eradication of HIV/AIDS (to Terumasa Ikeda); and Joint Usage/Research Center program of Institute for Frontier Life and Medical Sciences, Kyoto University (to Kei Sato).

References

1 Cele, S. *et al.* SARS-CoV-2 Omicron has extensive but incomplete escape of Pfizer BNT162b2 elicited neutralization and requires ACE2 for infection. *medRxiv*, 2021.2012.2008.21267417, doi:10.1101/2021.12.08.21267417 (2021).

2 Dejnirattisai, W. *et al.* Reduced neutralisation of SARS-COV-2 Omicron-B.1.1.529 variant by post-immunisation serum. *medRxiv*, 2021.2012.2010.21267534, doi:10.1101/2021.12.10.21267534 (2021).

3 Mlcochova, P. *et al.* SARS-CoV-2 B.1.617.2 Delta variant replication and immune evasion. *Nature* **599**, 114-119, doi:10.1038/s41586-021-03944-y (2021).

4 Saito, A. *et al.* Enhanced fusogenicity and pathogenicity of SARS-CoV-2 Delta P681R mutation. *Nature*, doi:10.1038/s41586-021-04266-9 (2021).

5 Peacock, T. P. *et al.* The furin cleavage site in the SARS-CoV-2 spike protein is required for transmission in ferrets. *Nat Microbiol*, doi:10.1038/s41564-021-00908-w (2021).

6 Meng, B. *et al.* Recurrent emergence and transmission of a SARS-CoV-2 spike deletion H69/V70 and role in Alpha Variant B.1.1.7. *Cell reports*, doi:https://doi.org/10.1016/j.celrep.2021.109292 (2021).

7 Mlcochova, P. *et al.* SARS-CoV-2 B.1.617.2 Delta variant replication and immune evasion. *Nature*, doi:10.1038/s41586-021-03944-y (2021).

8 Hoffmann, M. *et al.* SARS-CoV-2 Cell Entry Depends on ACE2 and TMPRSS2 and Is Blocked by a Clinically Proven Protease Inhibitor. *Cell* **181**, 271-280 e278, doi:10.1016/j.cell.2020.02.052 (2020).

9 Papa, G. *et al.* Furin cleavage of SARS-CoV-2 Spike promotes but is not essential for infection and cell-cell fusion. *PLoS pathogens* **17**, e1009246, doi:10.1371/journal.ppat.1009246 (2021).

10 Cattin-Ortolá, J. *et al.* Sequences in the cytoplasmic tail of SARS-CoV-2 Spike facilitate expression at the cell surface and syncytia formation. *bioRxiv*, 2020.2010.2012.335562, doi:10.1101/2020.10.12.335562 (2021).

11 Winstone, H. *et al.* The Polybasic Cleavage Site in SARS-CoV-2 Spike Modulates Viral Sensitivity to Type I Interferon and IFITM2. *Journal of virology* **95**, e02422-02420, doi:10.1128/jvi.02422-20 (2021).

12 Youk, J. *et al.* Three-Dimensional Human Alveolar Stem Cell Culture Models Reveal Infection Response to SARS-CoV-2. *Cell Stem Cell* **27**, 905-919 e910, doi:10.1016/j.stem.2020.10.004 (2020).

13 Sachs, N. *et al.* Long-term expanding human airway organoids for disease modeling. *The EMBO journal* **38**, doi:10.15252/embj.2018100300 (2019).

14 Wyler, E. *et al.* Transcriptomic profiling of SARS-CoV-2 infected human cell lines identifies HSP90 as target for COVID-19 therapy. *iScience* **24**, 102151, doi:10.1016/j.isci.2021.102151 (2021).

15 Madissoon, E. *et al.* A spatial multi-omics atlas of the human lung reveals a novel immune cell survival niche. *bioRxiv*, 2021.2011.2026.470108, doi:10.1101/2021.11.26.470108 (2021).

16 Kemp, S. *et al.* Recurrent emergence and transmission of a SARS-CoV-2 Spike deletion H69/V70. *bioRxiv*, 2020.2012.2014.422555, doi:10.1101/2020.12.14.422555 (2021).

17 Cathcart, A. L. *et al.* The dual function monoclonal antibodies VIR-7831 and VIR-7832 demonstrate potent in vitro and in vivo activity against SARS-CoV-2. *bioRxiv*, 2021.2003.2009.434607, doi:10.1101/2021.03.09.434607 (2021).

18 Katoh, K. & Standley, D. M. MAFFT multiple sequence alignment software version 7: improvements in performance and usability. *Mol Biol Evol* **30**, 772-780, doi:10.1093/molbev/mst010 (2013).

19 Jumper, J. *et al.* Highly accurate protein structure prediction with AlphaFold. *Nature* **596**, 583-589, doi:10.1038/s41586-021-03819-2 (2021).

20 Goddard, T. D. *et al.* UCSF ChimeraX: Meeting modern challenges in visualization and analysis. *Protein Science* **27**, 14-25 (2018).

21 Rihn, S. J. *et al.* A plasmid DNA-launched SARS-CoV-2 reverse genetics system and coronavirus toolkit for COVID-19 research. *PLoS Biol* **19**, e3001091, doi:10.1371/journal.pbio.3001091 (2021).

22 Vermeire, J. *et al.* Quantification of reverse transcriptase activity by real-time PCR as a fast and accurate method for titration of HIV, lenti- and retroviral vectors. *PloS one* **7**, e50859-e50859, doi:10.1371/journal.pone.0050859 (2012).

23 Kodaka, M. *et al.* A new cell-based assay to evaluate myogenesis in mouse myoblast C2C12 cells. *Experimental cell research* **336**, 171-181 (2015).

24 Papa, G. *et al.* Furin cleavage of SARS-CoV-2 Spike promotes but is not essential for infection and cell-cell fusion. *PLoS Pathogens* **17**, e1009246 (2021).

25 Buchrieser, J. *et al.* Syncytia formation by SARS-CoV-2-infected cells. *The EMBO journal* **39**, e106267 (2020).

26 Itokawa, K., Sekizuka, T., Hashino, M., Tanaka, R. & Kuroda, M. Disentangling primer interactions improves SARS-CoV-2 genome sequencing by multiplex tiling PCR. *PLoS One* **15**, e0239403, doi:10.1371/journal.pone.0239403 (2020).

27 Bolger, A. M., Lohse, M. & Usadel, B. Trimmomatic: a flexible trimmer for Illumina sequence data. *Bioinformatics* **30**, 2114-2120, doi:10.1093/bioinformatics/btu170 (2014).

28 Langmead, B. & Salzberg, S. L. Fast gapped-read alignment with Bowtie 2. *Nat Methods* **9**, 357-359, doi:10.1038/nmeth.1923 (2012).

29 Chen, S. *et al.* Gencore: an efficient tool to generate consensus reads for error suppressing and duplicate removing of NGS data. *BMC Bioinformatics* **20**, 606, doi:10.1186/s12859-019-3280-9 (2019).

30 Thorvaldsdottir, H., Robinson, J. T. & Mesirov, J. P. Integrative Genomics Viewer (IGV): high-performance genomics data visualization and exploration. *Brief Bioinform* **14**, 178-192, doi:10.1093/bib/bbs017 (2013).

31 Motozono, C. *et al.* SARS-CoV-2 spike L452R variant evades cellular immunity and increases infectivity. *Cell Host Microbe* **29**, 1124-1136, doi:10.1016/j.chom.2021.06.006 (2021).

32 Matsuyama, S. *et al.* Enhanced isolation of SARS-CoV-2 by TMPRSS2-expressing cells. *Proc Natl Acad Sci U S A* **117**, 7001-7003, doi:10.1073/pnas.2002589117 (2020).

33 Kimura, I. *et al.* SARS-CoV-2 Lambda variant exhibits higher infectivity and immune resistance. *BioRxiv*, 454085 (2021).

The Genotype to Phenotype Japan (G2P-Japan) Consortium members

Ryoko Kawabata[16], Nanami Morizako[16] , Kenji Sadamasu[17], Hiroyuki Asakura[17], Mami Nagashima[17], Kazuhisa Yoshimura[17], Jumpei Ito[18], Izumi Kimura[18], Keiya Uriu[18], Yusuke Kosugi[18], Mai Suganami[18], Akiko Oide[18], Miyabishara Yokoyama[18], Mika Chiba[18] , Akatsuki Saito[31], Erika P Butlertanaka[31], Yuri L Tanaka[31], Terumasa Ikeda[32], Chihiro Motozono[32], Hesham Nasser[32], Ryo Shimizu[32], Yue Yuan[32], Kazuko Kitazato[32], Haruyo Hasebe[32] , So Nakagawa[33], Jiaqi Wu[33], Miyoko Takahashi[33], Takasuke Fukuhara[34], Kenta Shimizu[34], Kana Tsushima[34], Haruko Kubo[34], Yasuhiro Kazuma[35], Ryosuke Nomura[35], Yoshihito Horisawa[35], Kayoko Nagata[35], Yugo Kawai[35], Yohei Yanagida[35], Yusuke Tashiro[35], Kenzo Tokunaga[36], Seiya Ozono[36]

[31]University of Miyazaki, Miyazaki, Japan
[32]Kumamoto University, Kumamoto, Japan
[33]Tokai University, Tokyo, Japan
[34]Hokkaido University, Sapporo, Japan
[35]Kyoto University, Kyoto, Japan
[36]National Institute of Infectious Diseases, Tokyo, Japan

The CITIID-NIHR BioResource COVID-19 Collaboration

Stephen Baker[1,2], Gordon Dougan[1,2] , Christoph Hess[2], Nathalie Kingston[9], Paul J. Lehner[1,2], Paul A. Lyons[1,2], Nicholas J. Matheson[1,2], Willem H. Owehand[22], Caroline Saunders[21], Charlotte Summers[2] , James E.D. Thaventhiran[2], Mark Toshner[2], Michael P. Weekes[2], Patrick Maxwell[37], Ashley Shaw[37]

Ashlea Bucke[38], Jo Calder[38], Laura Canna[38], Jason Domingo[38], Anne Elmer[38], Stewart Fuller[38], Julie Harris[38], Sarah Hewitt[38], Jane Kennet[38], Sherly Jose[38], Jenny Kourampa[38],

Anne Meadows[38], Criona O'Brien[38], Jane Price[38], Cherry Publico[38], Rebecca Rastall[38], Carla Ribeiro[38], Jane Rowlands[38], Valentina Ruffolo[38], Hugo Tordesillas[38], Ben Bullman[1], Benjamin J. Dunmore[2], Stuart Fawke[39], Stefan Gräf[2], Josh Hodgson[3], Christopher Huang[3], Kelvin Hunter[2,], Emma Jones[31], Ekaterina Legchenko[2], Cecilia Matara[2], Jennifer Martin[2], Federica Mescia[2], Ciara O'Donnell[2], Linda Pointon[2], Nicole Pond[2], Joy Shih[2], Rachel Sutcliffe[2], Tobias Tilly[2], Carmen Treacy[2], Zhen Tong[2], Jennifer Wood[2], Marta Wylot[2], Laura Bergamaschi[2], Ariana Betancourt[2], Georgie Bower[2], Chiara Cossetti[2,], Aloka De Sa[2], Madeline Epping[2], Stuart Fawke[2], Nick Gleadall[2], Richard Grenfell[2], Andrew Hinch[2], Oisin Huhn[39], Sarah Jackson[2], Isobel Jarvis[2], Ben Krishna[2], Daniel Lewis[3], Joe Marsden[3], Francesca Nice[41], Georgina Okecha[3], Ommar Omarjee[2], Marianne Perera[2], Martin Potts[2], Nathan Richoz[2], Veronika Romashova[2], Natalia Savinykh Yarkoni[3], Rahul Sharma[3], Luca Stefanucci[2], Jonathan Stephens[22], Mateusz Strezlecki[2], Lori Turner[2], Eckart M.D.D. De Bie[2], Katherine Bunclark[2], Masa Josipovic[2], Michael Mackay[2], Federica Mescia[2], Alice Michael[27], Sabrina Rossi[37], Mayurun Selvan[3], Sarah Spencer[15], Cissy Yong[37], John Allison[9], Helen Butcher[9,40], Daniela Caputo[9,40], Debbie Clapham-Riley[9,40], Eleanor Dewhurst[9,40], Anita Furlong[9,40], Barbara Graves[9,40], Jennifer Gray[9,40], Tasmin Ivers[9,40], Mary Kasanicki[9,30], Emma Le Gresley[9,40], Rachel Linger[9,40], Sarah Meloy[9,40], Francesca Muldoon[9,40], Nigel Ovington[9], Sofia Papadia[9,40], Isabel Phelan[9,40], Hannah Stark[9,40], Kathleen E Stirrups[22,12], Paul Townsend[40], Neil Walker[40], Jennifer Webster[9,40], Ingrid Scholtes[40], Sabine Hein[40], Rebecca King[40]

[37] Cambridge University Hospitals NHS Trust, Cambridge UK.

[38]Cambridge Clinical Research Centre, NIHR Clinical Research Facility, Cambridge University Hospitals NHS Foundation Trust, Addenbrooke's Hospital, Cambridge CB2 0QQ, UK

[39]Department of Biochemistry, University of Cambridge, Cambridge, CB2 1QW, UK

[40]University of Cambridge, Cambridge Biomedical Campus, Cambridge CB2 0QQ, UK

Ecuador-COVID19 Consortium

Paúl Cárdenas[uuu], Erika Muñoz[uuu], Veronica Barragan[uuu], Michelle Grunauer [vvv], Bernardo Gutierrez [www], Juan José Guadalupe [www], Juan Carlos Fernández-Cadena [xxx], Derly Andrade-Molina [yyy], Manuel Baldeon [zzz], Andrea Pinos [ooo]

[uuu] Universidad San Francisco de Quito, COCIBA, Instituto de Microbiología, Cumbaya EC1702, Ecuador
[vvv] Universidad San Francisco de Quito, COCSA, Escuela de Medicina, Cumbaya EC1702, Ecuador
[www] Universidad San Francisco de Quito, COCIBA, Laboratorio de Biotecnología Vegetal, Cumbaya EC1702, Ecuador
[xxx] Laboratorio INTERLAB, Guayaquil EC09, Ecuador
[yyy] Universidad Espíritu Santo, Laboratorio de Omicas, Guayaquil, EC09, Ecuador
[zzz] Universidad Internacional del Ecuador, Facultad de Ciencias Médicas, de la Salud y la Vida, Quito EC1701, Ecuador
[ooo] Centros Médicos Dr. Marco Albuja, Quito EC1701, Ecuador

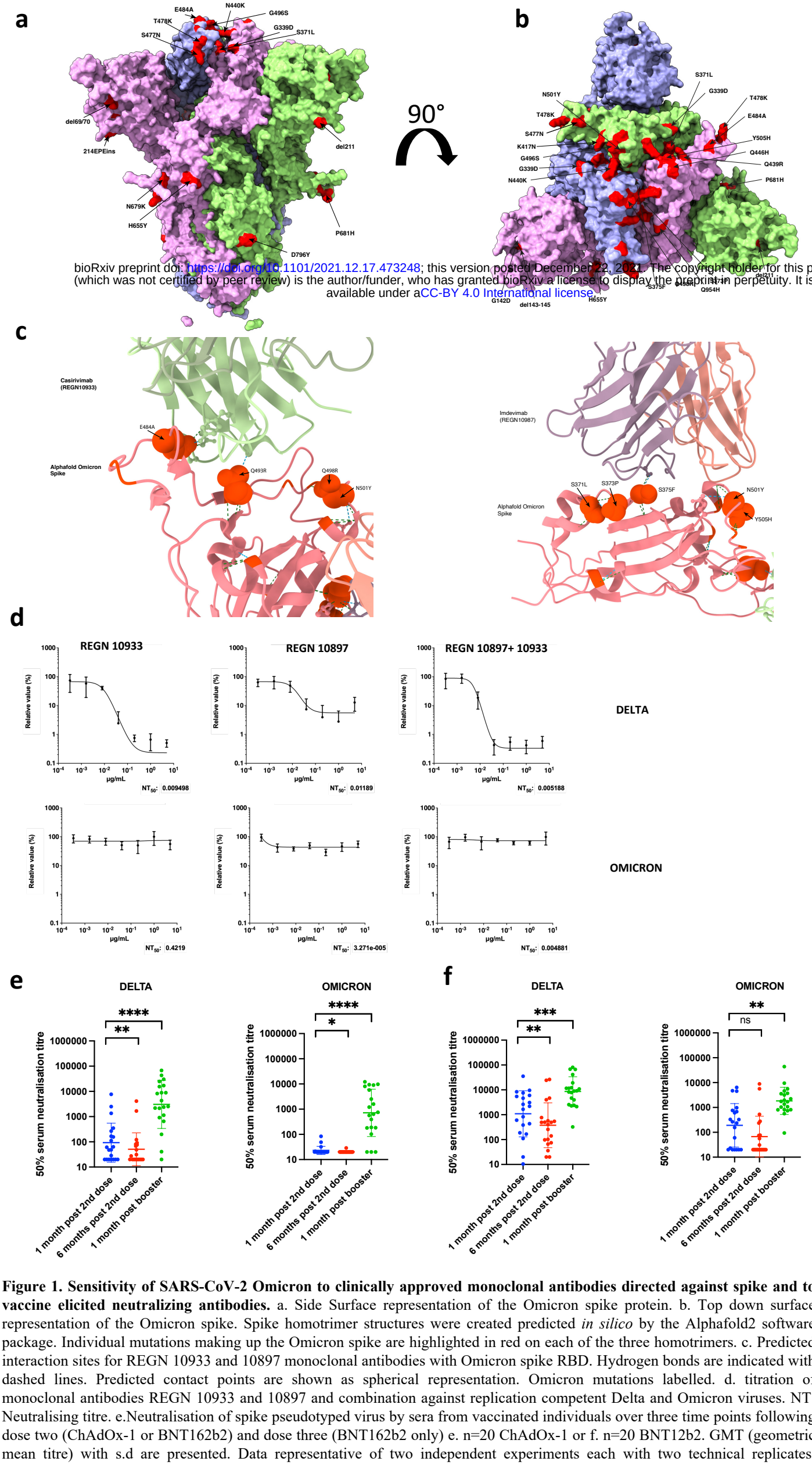

Figure 1. Sensitivity of SARS-CoV-2 Omicron to clinically approved monoclonal antibodies directed against spike and to vaccine elicited neutralizing antibodies. a. Side Surface representation of the Omicron spike protein. b. Top down surface representation of the Omicron spike. Spike homotrimer structures were created predicted *in silico* by the Alphafold2 software package. Individual mutations making up the Omicron spike are highlighted in red on each of the three homotrimers. c. Predicted interaction sites for REGN 10933 and 10897 monoclonal antibodies with Omicron spike RBD. Hydrogen bonds are indicated with dashed lines. Predicted contact points are shown as spherical representation. Omicron mutations labelled. d. titration of monoclonal antibodies REGN 10933 and 10897 and combination against replication competent Delta and Omicron viruses. NT: Neutralising titre. e.Neutralisation of spike pseudotyped virus by sera from vaccinated individuals over three time points following dose two (ChAdOx-1 or BNT162b2) and dose three (BNT162b2 only) e. n=20 ChAdOx-1 or f. n=20 BNT12b2. GMT (geometric mean titre) with s.d are presented. Data representative of two independent experiments each with two technical replicates. **p<0.01, *** p<0.001, ****p<0.0001 Wilcoxon matched-pairs signed rank test, ns not significant.

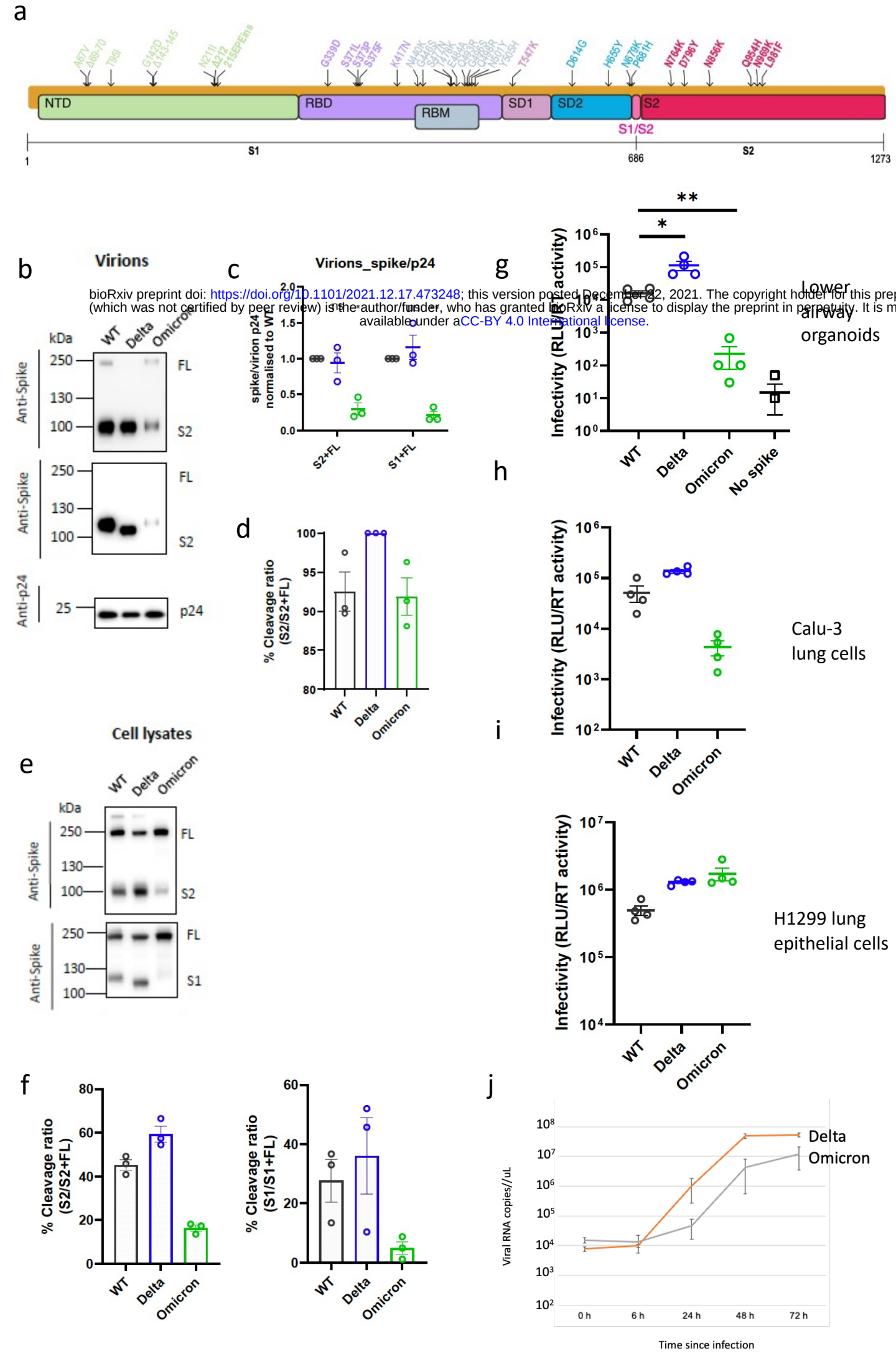

Figure 2: SARS-CoV-2 Omicron Variant spike mediated entry efficiency and replication. a. Graphical representation of Omicron spike mutations present in expression plasmid used. Mutations coloured according to location in spike; bold mutations are novel to this lineage and have not been identified in previous variants of concern (VOCs). **b.** western blots of pseudotyped virus (PV) virions from 293T producer cells following transfection with plasmids expressing lentiviral vectors and SARS-CoV-2 S plasmids. (WT- Wuhan-1 with D614G), probed with antibodies for HIV-1 p24 and SARS-Cov-2 S2 (top) and S1 (bottom). **c-d.** quantification of western blots showing c. ratio of spike:p24 in virions, d. ratio of S2:total spike**. e-f.** Western blot of cell lysates used to produce virions with quantification of S2 and S1 ratios to total spike. **g, h, i.** Single round infectivity using PV on lung alveolar organoids, Calu-3 lung cells, and H1299 lung epithelial cells. **j**. Spreading infection by replication competent Omicron versus Delta variant over 72 hours in Calu-3 lung cell line.

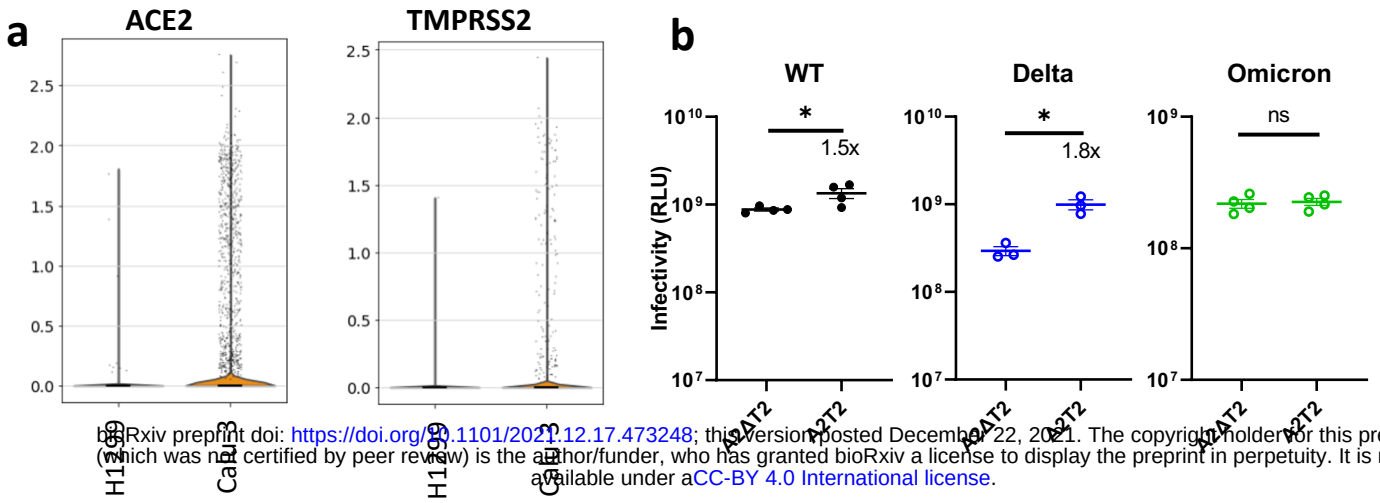

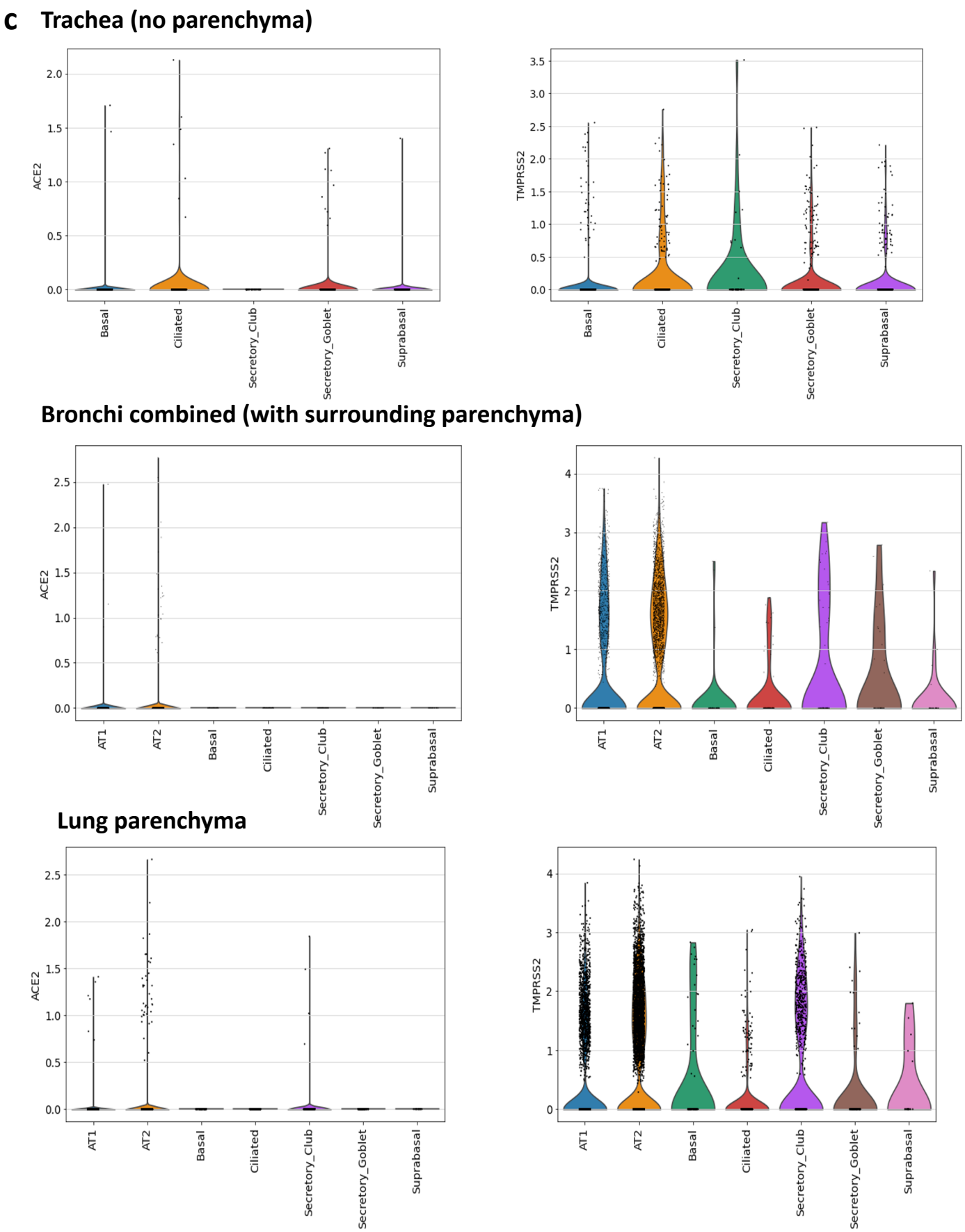

Figure 3: SARS-CoV-2 Omicron Variant spike uses TMPRSS2 **receptor inefficiently for entry.** TMPRSS2 is expressed at higher levels in epithelial cells of the human alveoli compared to the airway and is differentially expressed in Calu-3 versus H1299 lung cell lines. **a**. Log-normalised expression of ACE2 and TMPRSS2 genes in single-cell RNA-seq data from human non-small cell lung cancer cell lines with epithelial origin (H1299 and Calu-3) **b.** Entry of PV expressing spike in 293T cells transduced to overexpress ACE2 and (i) depleted for TMPRSS2 (A2 ▵ T2) or (ii) overexpressing TMPRSS2. Data are representative of two independent experiments. C**.** Log-normalised expression of ACE2 and TMPRSS2 genes in single-nuclei RNAseq data from human alveolar (AT1 - alveolar type 1, AT2 - alveolar type 2 pneumocytes) and airway epithelial cells (basal, suprabasal, goblet and

a

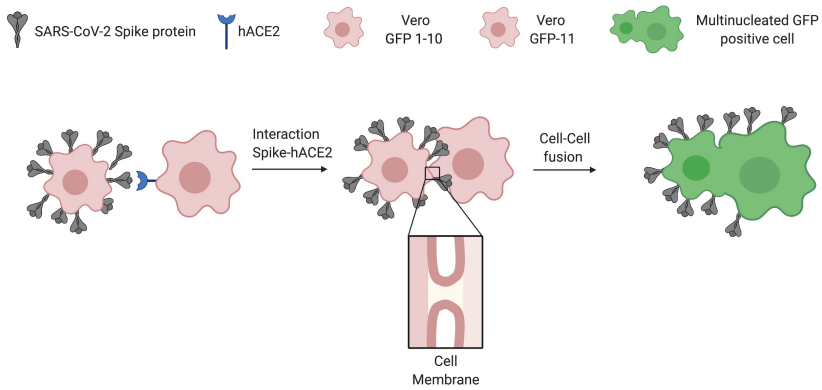

b

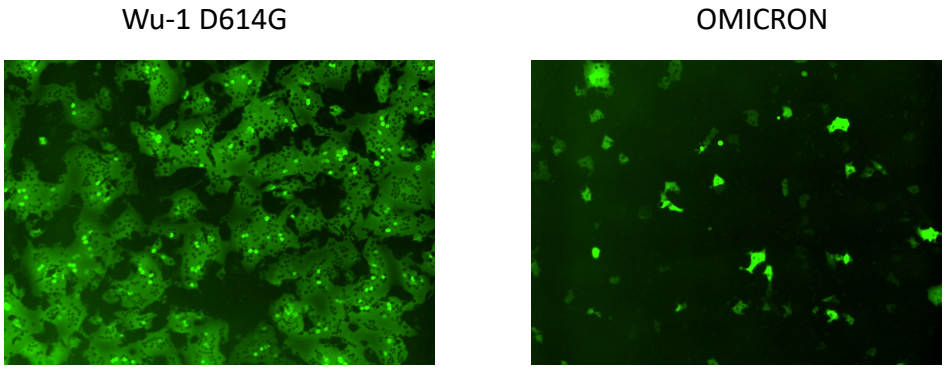

c

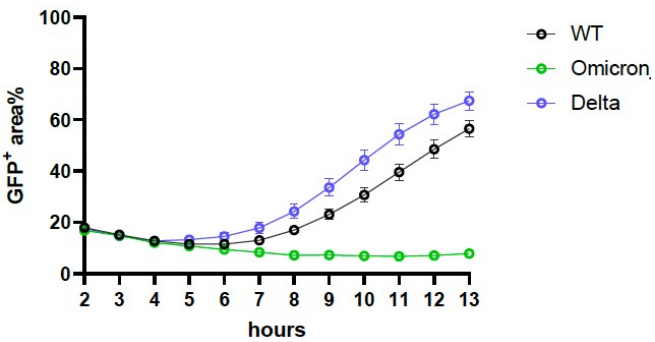

Figure 4: SARS-CoV-2 Omicron variant spike confers impaired cell-cell fusion activity. a. Schematic of cell-cell fusion assay. **b.** Reconstructed images at 16 hours of GFP+ syncytia. **c.** Quantification of cell-cell fusion kinetics showing percentage of green area to total cell area over time (WT is Wuhan-1 D614G). Mean is plotted with error bars representing SEM. Data are representative of at least two independent experiments.

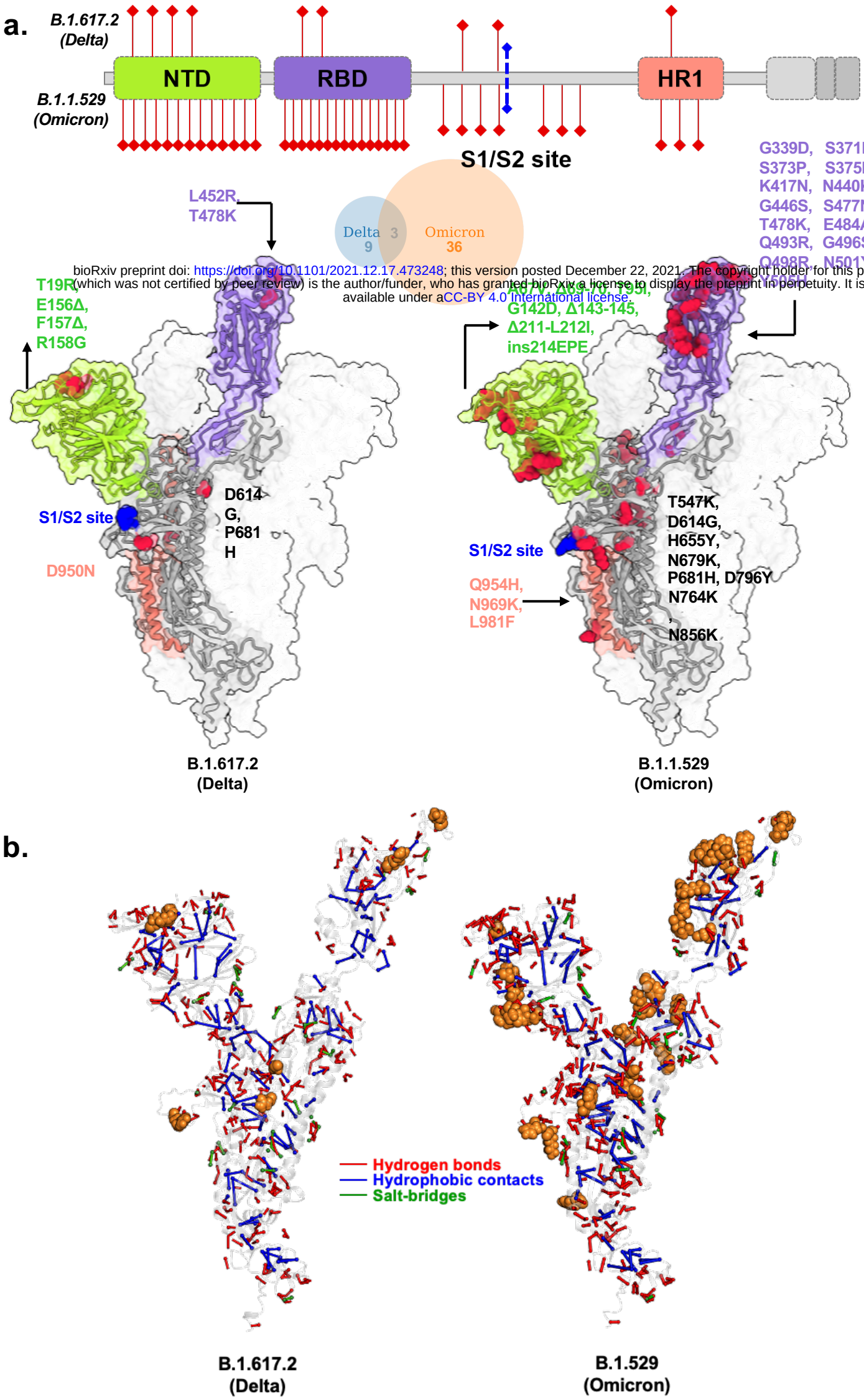

Supplementary Figure 1: Structural models of SARS-CoV-2 Delta and Omicron spike variants and their corresponding protein intramolecular network. a. Variant structures for Delta and omicron of spike protein displaying mutational sites in red color. The schematic highlights differences in domain-wise mutations across protein length. b. The non-covalent interactions, including hydrogen bonds, hydrophobic contacts, and salt bridges are shown for Delta and omicron variants in red, blue, and green, respectively. The interactions were calculated on 100 ns molecular dynamics simulation and interactions with >50% persistence are shown. For clarity only unique hydrogen bonds specific to each variant spike protein are marked in red for one chain. The mutations present in Delta and Omicron are marked in yellow spheres.

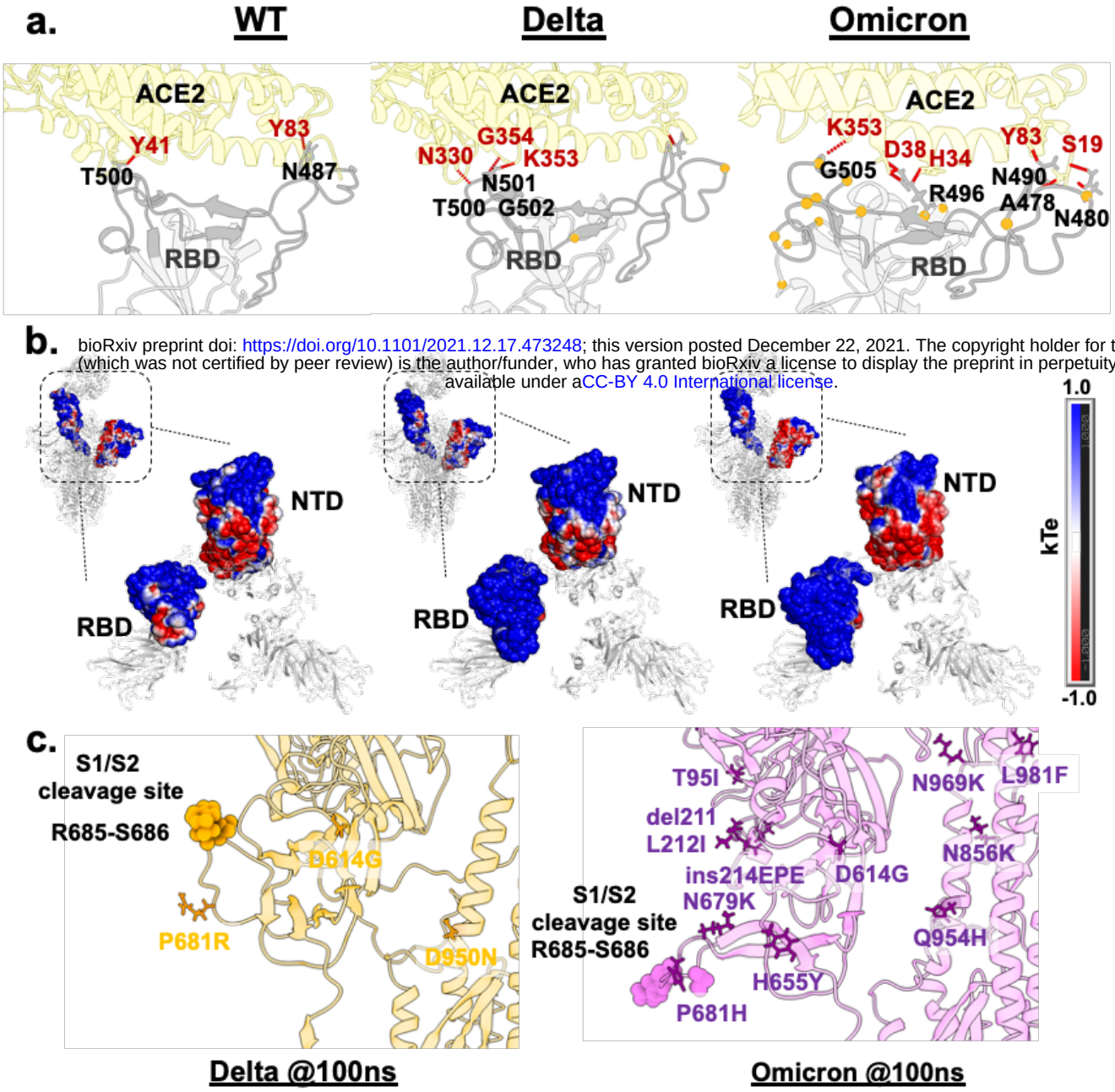

Supplementary Figure 2. Evaluating interaction surfaces of SARS-CoV-2 spike protein based on molecular dynamics simulations. a. The binding interface of ACE2 and RBD region of spike protein is shown for wuhan-1, Delta, and Omicron. The hydrogen bonds in each model are shown in red color with participating residues marked in black. The mutations present in the RBD region are highlighted in yellow color **b.** Electrostatic surface of the spike NTD and RBD regions is illustrated, with positive and negative charge potential shown in blue, and red, respectively. **c.** The zoomed image of proteolytic cleavage site loop harboring S1/S2 site (R685-S686) is shown in vdw spheres for Delta (orange) and Omicron (purple) variants. The structural region in proximity is shown to highlight mutation sites shown in stick representation.

a

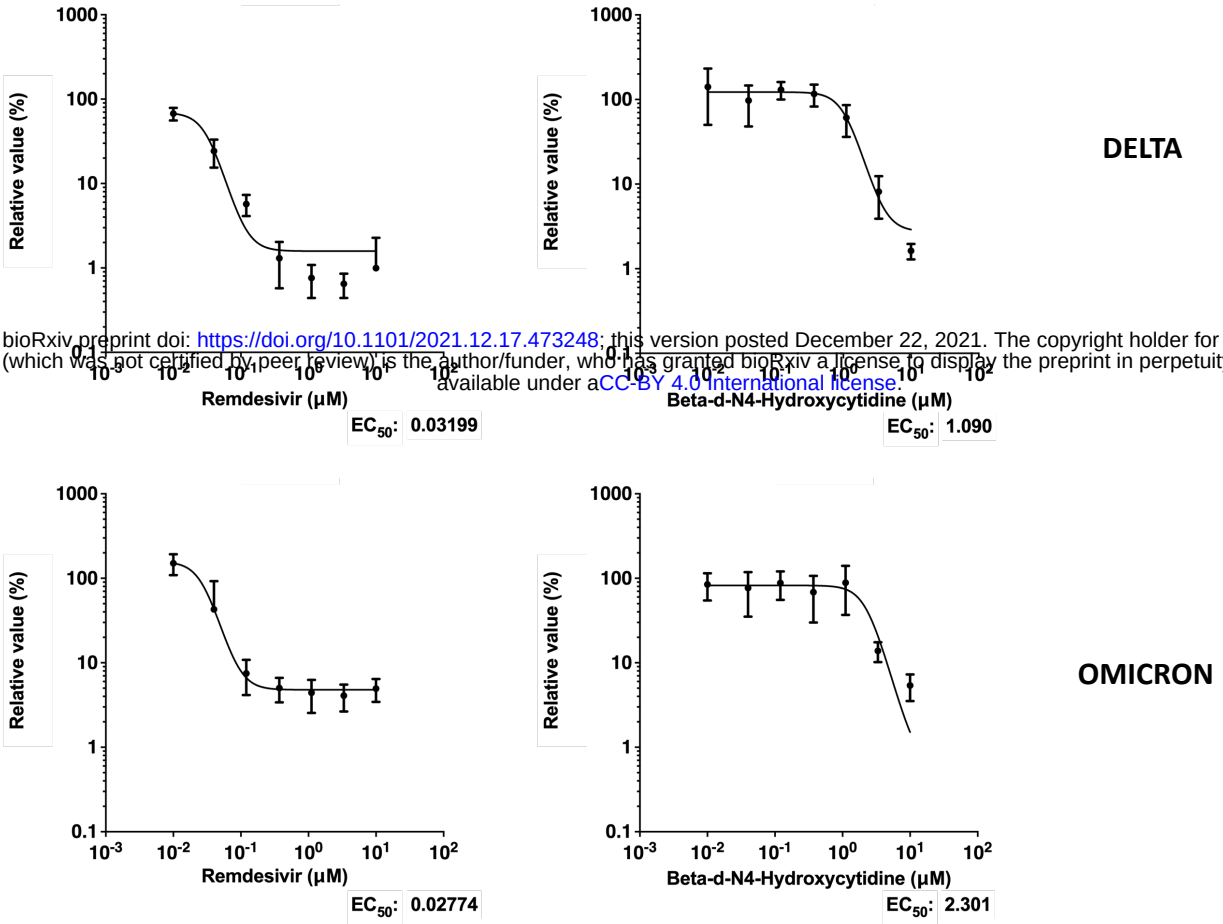

b

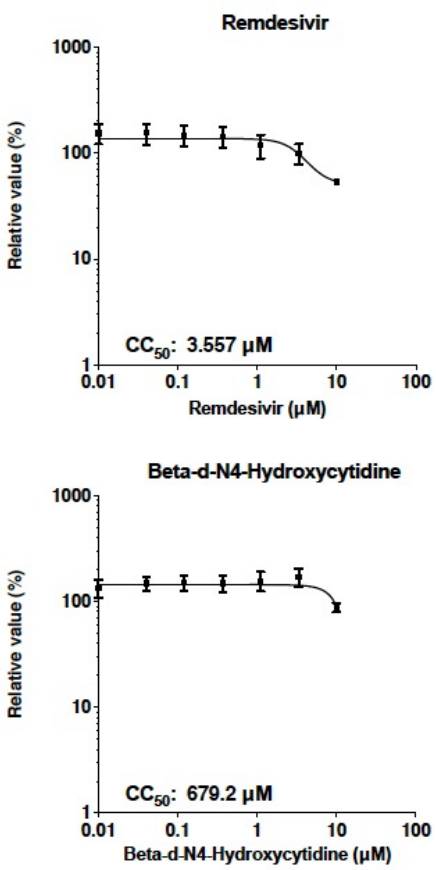

Supplementary Figure 3 : **Sensitivity of replication competent SARS-CoV-2 Omicron and Delta variants to clinically approved direct acting antiviral molecules remdesivir and the active metabolite of molnupiravir.** HOS cells overexpressing ACE2 and TMPRSS2 were used and a viral input of 1000TCID50 was used (TCID50 measured using VeroE6/TMPRSS2 cells). **a.** Dose-response curves. Infection as measured by viral RNA copies relative to the no drug control (100%) is plotted on the y axis with serial drug dilution on the x axis. EC50 is indicated for each panel and calculated in GraphPad Prism. **b**. toxicity assay showing relative cell viability at a range of drug doses. Data are representative of two independent experiments.

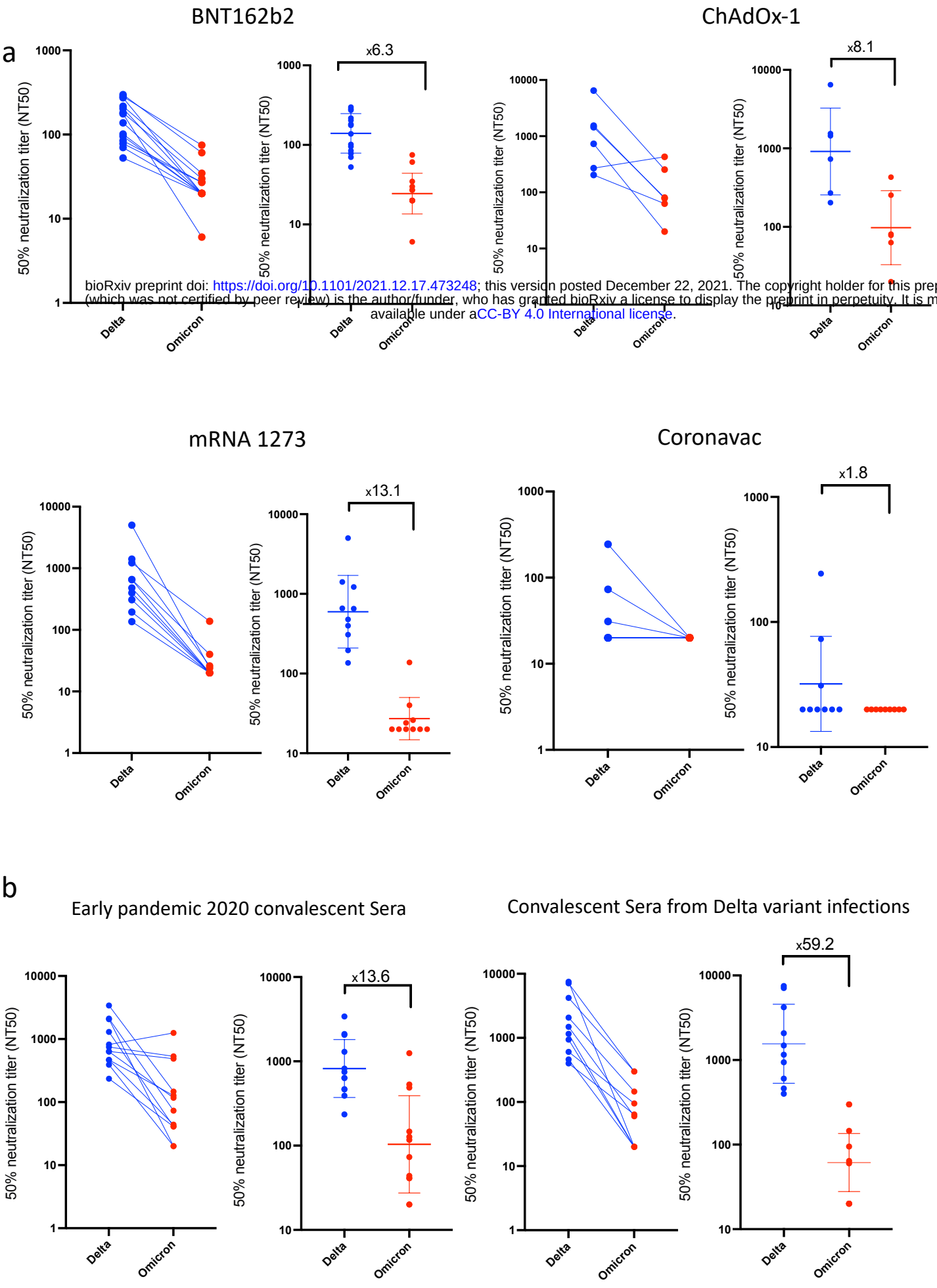

Supplementary Figure 4: a. Neutralisation of replication competent Delta and Omicron viruses by sera from vaccinated individuals following dose two of ChAdOx-1, BNT162b2, mRNA 1273, and Coronavac vaccines**. b.** neutralization of live viruses by sera derived from recovered individuals following infection in early 2020 or with confirmed Delta infection. Data are representative of two independent experiments